


**Brownian motors powered by nonreciprocal interactions**Bao-quan Ai <sup>1,2</sup><sup>1</sup>*Key Laboratory of Atomic and Subatomic Structure and Quantum Control (Ministry of Education), Guangdong Basic Research Center of Excellence for Structure and Fundamental Interactions of Matter, School of Physics, South China Normal University, Guangzhou 510006, People's Republic of China*<sup>2</sup>*Guangdong Provincial Key Laboratory of Quantum Engineering and Quantum Materials, and Guangdong-Hong Kong Joint Laboratory of Quantum Matter, South China Normal University, Guangzhou 510006, People's Republic of China*

(Received 11 August 2023; accepted 28 November 2023; published 21 December 2023)

Traditional models for molecular (Brownian) motors predominantly depend on nonequilibrium driving, while particle interactions rigorously adhere to Newton's third law. However, numerous living and natural systems at various scales seem to defy this well-established law. In this study, we investigated the transport of mixed Brownian particles in a two-dimensional ratchet potential with nonreciprocal interactions. Our findings reveal that these nonreciprocal interactions can introduce a zero-mean nonequilibrium driving force. This force is capable of disrupting the thermodynamic equilibrium and inducing directed motion. The direction of this motion is determined by the asymmetry of the potential. Interestingly, the average velocity is a peaked function of the degree of nonreciprocity, while the effective diffusion consistently increases with the increase of nonreciprocity. There exists an optimal temperature or packing fraction at which the average velocity reaches its maximum value. We share a mechanism for particle rectification, devoid of particle-autonomous nonequilibrium drive, with potential usage in systems characterized by nonreciprocal interactions.

DOI: [10.1103/PhysRevE.108.064409](https://doi.org/10.1103/PhysRevE.108.064409)**I. INTRODUCTION**

Nature utilizes an intriguing mechanism known as molecular motors [1] to facilitate directed transport within cells and propel bacteria in dynamic ecosystems. These molecular motors, protein complexes, convert differences in chemical potential between reactants and products into directed motion or work against a gradient. Despite their extensive diversity, all molecular motors share a common principle of exploiting Brownian fluctuations, albeit through various mechanisms. Being essential for biological processes, these motors are driven by Brownian motion and nonequilibrium driving forces, which is often conceptualized through a model known as the Brownian ratchet. This model is believed to underpin the functionality of several inherent biological motors, such as the  $F_1F_0$  ATPase [2], and its validity has been experimentally demonstrated in synthetic microscale systems, including artificial molecular motors created by organic chemical synthesis [3,4].

The term Brownian ratchet refers to a group of models for directed transport that utilize Brownian motion, rectified via energy input [5–10]. The ratchet effect emerges when a system is shifted from thermodynamic equilibrium and the system's symmetries are violated. Ratchet devices are classified into four categories based on the type of nonequilibrium driving involved. (i) Rocking ratchets [11–23], where unbiased external forces perturb thermodynamic equilibrium, inducing directed transport in asymmetric potentials. (ii) Flashing ratchets [24–29], where directed motion is instigated by the random oscillation of an asymmetric potential between two or more states, or by the time modulation of the potential. (iii) Correlation ratchets [30–34], where the time correlation or spontaneous collective motion instigates directed transport.

(iv) Self-propelled ratchets [35–55], where self-propelled forces disturb thermodynamic equilibrium, effectuating net transport in asymmetric structures. For instance, the ratchet's broken spatial symmetry rectifies the self-propelled motion of the particles [35], leading to a net current. Key conditions for the directed motion of Brownian particles to arise from these ratchet systems encompass nonequilibrium driving and either temporal or spatial asymmetry.

The conventional ratchet model demands nonequilibrium driving, and particle interactions adhere to Newton's third law. However, numerous living and natural systems across multiple scales appear to defy this law. Specifically, the principle of action-reaction symmetry might be violated for mesoscopic particles when their nonreciprocal interactions are regulated by a nonequilibrium environment [56–63]. This asymmetry ensues when the environment moves relative to the particles or when a system of particles is made up of different species whose interaction with the environment is in nonequilibrium. Examples of this exist in nature, ranging from bacteria interactions [64] at the microscale to animal herd dynamics [65] at the macroscale. In artificial systems, the use of magnetic microdisks can selectively disrupt action-reaction reciprocity by exploiting fluid-mediated hydrodynamic interactions [66]. From a theoretical perspective, the temporal-dependent nonreciprocal interactions can induce sustained active motion [67], akin to the patterns manifested in traditional active particle models. Therefore, a crucial question arises: How do nonreciprocal interactions affect the directed motion of Brownian particles? Specifically, does particle-autonomous nonequilibrium driving remain a necessary requirement for the functionality of a Brownian motor in the presence of nonreciprocal interactions?

To address this, we analyzed the transport of a binary mixture of Brownian particles with nonreciprocal interactions in a two-dimensional ratchet potential. Our findings demonstrate that in the absence of particle-autonomous nonequilibrium driving, the nonreciprocal interactions between particles generate an interaction-dependent propulsive force. This force can break the thermodynamic equilibrium and induce the directed motion of Brownian particles in an asymmetric potential. The directional motion of Brownian particles is solely determined by the asymmetry of the potential. Moreover, we identified optimal parameters, including the packing fraction, degree of nonreciprocity, and temperature, at which the average velocity reaches its maximum value.

## II. MODEL AND METHODS

We consider a binary mixture of Brownian particles, consisting of equal proportions of species *A* and species *B*, confined within a two-dimensional box of size  $L_x \times L_y$ , and operating under periodic boundary conditions. Here, we consider that the interactions between the Brownian particles are nonreciprocal, thus violating Newton's third law. The position of particle *i* is represented by the coordinates  $\mathbf{r}_i \equiv (x_i, y_i)$  of its center. We neglected both hydrodynamic interactions among the particles and inertial terms. In the overdamped limit, the dynamics of particle *i* are described by the following overdamped Langevin equation:

$$\frac{d\mathbf{r}_i}{dt} = \mu \left[ \sum_{j \neq i} \mathbf{F}_{ij} + \mathbf{G}_i \right] + \sqrt{2\mu k_B T} \boldsymbol{\zeta}_i(t), \quad (1)$$

where  $T$  is the temperature,  $k_B$  the Boltzmann constant, and  $\mu$  the mobility.  $\boldsymbol{\zeta}_i(t)$  signifies a Gaussian white-noise random vector exhibiting zero mean and unit variance.

The substrate force  $\mathbf{G}_i = -\nabla V$  arises from the following two-dimensional ratchet potential:

$$V(x, y) = -V_0 \left[ \sin\left(\frac{2\pi x}{l_x}\right) + \frac{\Delta}{4} \sin\left(\frac{4\pi x}{l_x}\right) + \sin\left(\frac{2\pi y}{l_y}\right) \right], \quad (2)$$

where  $l_{x,y}$  is the substrate period and  $V_0$  is height of the potential. As for the potential, it demonstrates symmetry in the *y* direction but asymmetry in the *x* direction.  $\Delta$  manifests as the parameter responsible for any potential asymmetry along the *x* direction; when  $\Delta = 0$ , the potential is entirely symmetric.

Nonreciprocity is a common characteristic of both living and natural systems. Increasingly, it is being employed to modify the structure and dynamics of synthetic materials across a wide range of scales. In this study, we explore a category of nonreciprocal interactions as outlined in Ref. [57]. This interaction allows for an easily adjustable and continuous fluctuation of nonreciprocity. The pairwise force  $\mathbf{F}_{ij}(\mathbf{r})$ , exerted on particle *i* by particle *j*, takes the subsequent form as detailed in Ref. [57]:

$$\mathbf{F}_{ij}(\mathbf{r}) = \mathbf{F}_{ij}^C(\mathbf{r}) \times \begin{cases} 1 - g(r), & ij \in AB, \\ 1 + g(r), & ij \in BA, \\ 1, & ij \in AA \text{ or } BB, \end{cases} \quad (3)$$

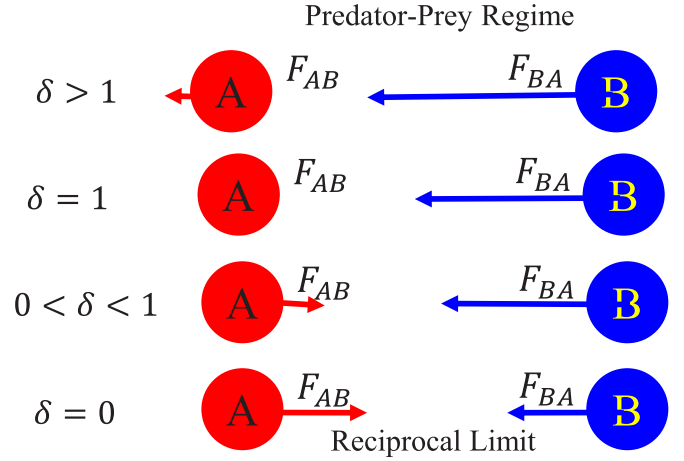


FIG. 1. Schematic representation of pairwise nonreciprocal interactions between species *A* and *B* for different  $\delta$ . The system operates under the reciprocal limit at  $\delta = 0$ , and transitions into a predator-prey regime when  $\delta > 1$ . When  $\delta \neq 0$ , an additional net force emerges in the interaction between two particles, which does not satisfy Newton's third law.

where  $\mathbf{F}_{ij}^C$  represents the conservative interaction force, abiding by Newton's third law, i.e.,  $\mathbf{F}_{ij}^C + \mathbf{F}_{ji}^C = 0$ . The function  $g(r)$  is a representation of nonreciprocity. Interactions between particles of the same species are entirely reciprocal ( $\mathbf{F}_{ij} = \mathbf{F}_{ji}^C$ ). However, interspecies interactions present both reciprocal  $\mathbf{F}_{ij}^R = \mathbf{F}_{ji}^C$  and nonreciprocal  $\mathbf{F}_{ij}^{NR} = \pm g(r) \times \mathbf{F}_{ij}^C$  components. The conservative interaction force,  $\mathbf{F}_{ij}^C = -\nabla U$  emerges from the corresponding truncated and shifted Lennard-Jones potential [68]

$$U(r) = \begin{cases} 4\epsilon \left[ \left(\frac{\sigma}{r}\right)^{12} - \left(\frac{\sigma}{r}\right)^6 + C_{\text{shift}} \right], & r \leq 2.5\sigma, \\ 0, & r > 2.5\sigma, \end{cases} \quad (4)$$

where the constants  $\epsilon$  and  $\sigma$  determine the energy unit and the nominal particle diameter, respectively. In this case, we choose the value of  $C_{\text{shift}} = \left(\frac{2}{5}\right)^6 - \left(\frac{2}{5}\right)^{12}$  so that the potential remains continuous at  $r = 2.5\sigma$ .

For simplicity, we consider a step nonreciprocity function defined as

$$g(r) = \begin{cases} \delta, & r \geq d_{\text{rec}}, \\ 0, & r < d_{\text{rec}}, \end{cases} \quad (5)$$

where  $\delta$  specifies the degree of nonreciprocity and  $d_{\text{rec}}$  represents a reciprocity diameter. All particle pairs exhibit strictly reciprocal repulsion within a separation distance of  $d_{\text{rec}}$ . Note that by setting  $d_{\text{rec}} > \sigma$ , we control the nonreciprocity only via the attractive part of the interaction without much loss of generality. Additionally, we confirm that accounting for nonreciprocity in both the attractive and repulsive components does not create a qualitative difference in the results. Therefore, for convenience, we set  $d_{\text{rec}} = 2^{1/6}\sigma$  in our study. The pairwise nonreciprocal interactions between different species are represented in Fig. 1. When  $\delta = 0$ , there exists no net force. For  $0 < \delta < 1$ , each species experiences a force of variable magnitude, with these forces continually opposing one another. Conversely, for  $\delta > 1$ , nonreciprocity results in

opposing forces that no longer counteract each other: a particle that exerts a repulsive (attractive) force will subsequently experience an attractive (repulsive) force. This phenomenon is reminiscent of the so-called predator-prey interaction witnessed in nature.

To quantify the ratchet effect, we measure the average velocity in the  $x$  direction. In the asymptotic long-time regime, the average velocity of the particle along the  $x$  direction can be obtained from the following formula:

$$V_x = \lim_{t \rightarrow \infty} \frac{\Delta X(t)}{t}, \quad (6)$$

where  $\Delta X(t) = \frac{1}{N} \sum_{i=1}^N \langle x_i(t) - x_i(0) \rangle$  is the average displacement of particles at time  $t$  along the  $x$  direction.  $x_i(t)$  is the center of mass of particle  $i$ . The symbol  $\langle \dots \rangle$  denotes an average over the random initial conditions and 100 stochastic trajectories are used to perform ensemble average.

In order to characterize the diffusion behavior of particles, we employ the time-dependent mean square displacement (MSD) which is defined as follows:

$$\text{MSD}(t) = \frac{1}{N} \left\langle \sum_i [\mathbf{r}'_i(t) - \mathbf{r}'_i(0)]^2 \right\rangle. \quad (7)$$

Here, the calculation is performed in the reference frame of the center of mass, denoted by  $\mathbf{r}_{cm} = \frac{1}{N} \sum_i \mathbf{r}_i$ , where  $\mathbf{r}'_i = \mathbf{r}_i - \mathbf{r}_{cm}$ . The ensemble average, denoted by the brackets, is calculated under steady-state conditions. Accordingly, the effective diffusion coefficient is derived from the long-time behavior and expressed as  $D_{\text{eff}} = \lim_{t \rightarrow \infty} \frac{\text{MSD}(t)}{4t}$ .

To integrate Eq. (1), we employ the Euler algorithm with a step time of  $10^{-5}$ . The total integration time is  $10^5$ , which is sufficient to ensure that the system can reach a nonequilibrium steady state. Particle positions are initialized using a uniform random distribution within the confining box. The particle density within the box is described by the packing fraction  $\phi = N\pi\sigma^2/(4L_xL_y)$ , which represents the ratio of the area occupied by particles to the total available area. In the simulations, we implemented periodic boundary conditions. We set  $L_x = 2L_y$ ,  $L_x = 2l_x$ , and  $L_y = 2l_y$  without loss of generality. Unless indicated otherwise, simulations are executed using the following parameters:  $k_B = 1$ ,  $\epsilon = 1$ ,  $\mu = 1$ ,  $V_0 = 0.5$ , and  $N = 1000$ . The robustness of the presented results has been confirmed under reasonable alterations of these parameters. It needs to be clarified that our work primarily focuses on the system being in the liquid phase.

### III. RESULTS AND DISCUSSION

We first discuss the implementation of rectification conditions for Brownian particles in our model. The ratchet mechanism necessitates two crucial components: (i) a nonequilibrium driving force, which disrupts thermal equilibrium and prevents directed transport due to the Second Law of Thermodynamics; and (ii) asymmetry, either temporal or spatial, which interrupts the left-right symmetry of the response. In the system under consideration, there is an absence of a particle-autonomous nonequilibrium drive. However, the nonreciprocal interactions embedded within our model produce a net force  $\mathbf{F}_{ij}^{\text{net}}(t) = \mathbf{F}_{ij}(t) + \mathbf{F}_{ji}(t)$  between particle  $i$

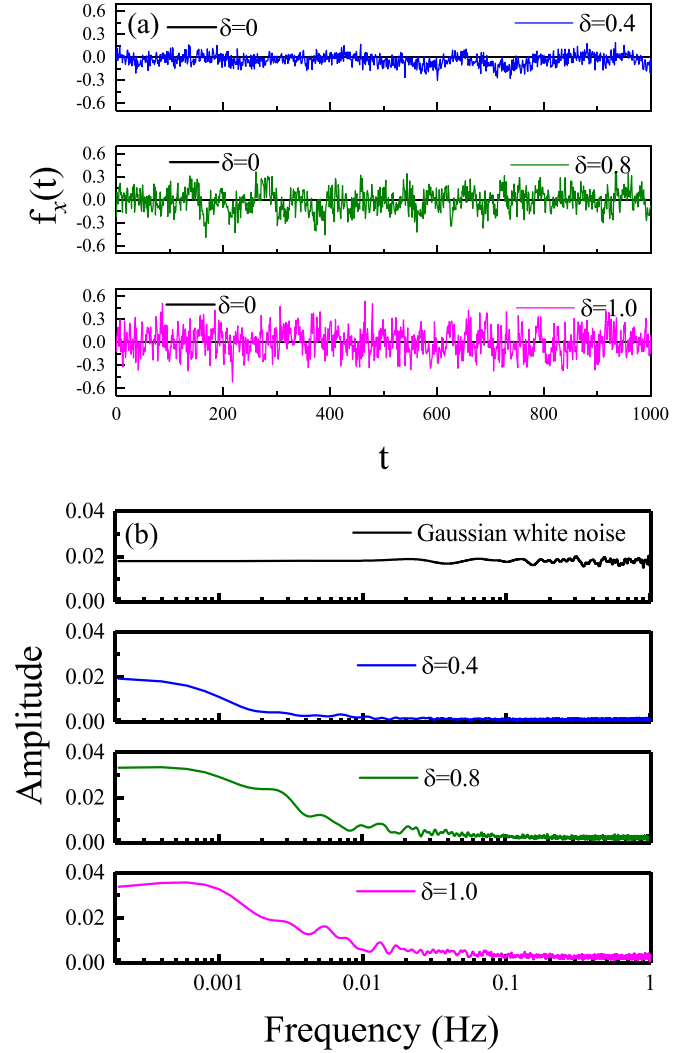


FIG. 2. (a) Plot illustrating the typical average net force  $f_x$  on a particle against time  $t$  for different  $\delta$ . The black solid line represents the case of reciprocity ( $\delta = 0$ ), indicating that in reciprocal situations,  $f_x$  is always zero. For nonreciprocal situations ( $\delta = 0.4, 0.8, 1.0$ ), a net random force appears. (b) Comparison of the power spectral density of  $f_x(t)$  for varying values of  $\delta$  with that of Gaussian white noise. The other parameters are  $\phi = 0.2$  and  $T = 0.3$ .

and  $j$ , which can be treated as an internally generated active force. For the purposes of our discussion, we define the average force impacting each particle at a given time  $t$ , derived from nonreciprocal interactions, as  $\mathbf{f}(t) = \frac{1}{N} \sum \mathbf{F}_{ij}^{\text{net}}(t)$ . This force is determined by particle configurations as well as the degree of nonreciprocity  $\delta$ . In the scenario of reciprocity, all action and reaction forces are fully neutralized, leaving no net force. Consequently, the net force  $\mathbf{f}(t)$  always equals zero. In the nonreciprocal case, as particle configurations fluctuate randomly over time,  $\mathbf{f}(t)$  also exhibits randomness.

Figure 2(a) compares the time-dependent net force  $\mathbf{f}(t)$  in the  $x$  direction, specifically referred to as  $f_x(t)$ , acting on a particle under both reciprocal and nonreciprocal conditions at  $\phi = 0.2$  and  $T = 0.3$ . When  $\delta = 0.0$ , all particle interactions are purely reciprocal. In consequence, the magnitudes of the action and reaction forces are equal but are

directed oppositely, hence  $f_x(t)$  consistently equals zero (no nonequilibrium driving). If we consider nonreciprocal interactions (e.g.,  $\delta > 0$ ), the net force  $f_x(t)$  fluctuates around zero, operating similarly to a nonequilibrium driving force. This oscillating force subsequently intensifies with an increase in  $\delta$ .

In order to examine the persistence of the net force  $f_x(t)$ , we computed its power spectral density as shown in Fig. 2(b), and compared it with that of Gaussian white noise. From the definition of the white noise via its covariance, the spectral density of Gaussian white noise appears uniform. Nevertheless, for nonreciprocal interactions, the spectral density of  $f_x(t)$  is dominated by the low-frequency component over the high-frequency one. The net force  $f_x(t)$  can be artificially decomposed into two components: Gaussian white noise and low-frequency ac drive. The persistent active motion, which resembles patterns observed in conventional active particle models, can potentially be induced by the latter constituent. As a result, the net force emerging from nonreciprocal interactions could act as a nonequilibrium drive. Note that the previous literature [69] has also demonstrated that nonreciprocal interactions can drive a system out of equilibrium. The subsequent section will focus on how this nonequilibrium drive leads to directional movement of Brownian particles within a ratchet potential.

Figure 3(a) depicts the relationship between the average velocity  $V_x$  and the asymmetric parameter  $\Delta$  for different  $\delta$  values at  $\phi = 0.2$  and  $T = 0.3$ . The average velocity  $V_x$  is found to be positive for  $\Delta > 0$ , zero at  $\Delta = 0$ , and negative for  $\Delta < 0$ . A qualitative explanation of this phenomenon is provided below. When  $\Delta > 0$ , the potential's left side from the minima exhibits steeper characteristics [as depicted in the top panel of Fig. 3(b)]. Consequently, it is more accessible for particles to move toward the sloped side than the steep side, resulting in an average rightward movement of particles ( $V_x > 0$ ). Conversely, when  $\Delta < 0$ , particles tend to move leftward on average ( $V_x < 0$ ). For  $\Delta = 0$ , the potential is entirely symmetric [as shown in the middle panel of Fig. 3(b)], leading to equal probabilities of particle movement to either side and the disappearance of directed motion. In the case of large  $\Delta$  limits, the potential barrier height increases to a point where particles get trapped in local minima, which in turn suppresses rectification. Hence, there exists an optimal value of  $\Delta$  at which  $V_x$  reaches its peak. Due to the perfectly antisymmetric relationship between  $V_x$  and  $\Delta$ , we will limit the discussion to only cases where  $\Delta > 0$ .

Figures 4(a) and 4(b) respectively represent the average velocity  $V_x$  and the effective diffusion coefficient  $D_{\text{eff}}/(\mu k_B T)$  as functions of the degree of nonreciprocity  $\delta$ . Upon comparison, it becomes clear that the relationships between  $V_x$  and  $D_{\text{eff}}/(\mu k_B T)$  in relation to  $\delta$  are substantially different. The former exhibits a peak relationship, whereas the latter demonstrates a monotonically increasing relationship. At  $T = 0$ , the dynamics become deterministic and once equilibrium is achieved, the particle configurations remain unchanged. The absence of a nonequilibrium drive implies no directed motion. Upon examination,  $V_x$  is observed to be a peaked function of  $\delta$ . This is explicable via an earlier discussion that revealed the nonequilibrium driving force  $f_x(t)$  to increment along with  $\delta$  (Fig. 2). Simultaneously, the effective diffusion coefficient  $D_{\text{eff}}/(\mu k_B T)$  also escalates with  $\delta$  [Fig. 4(b)]. This unveils

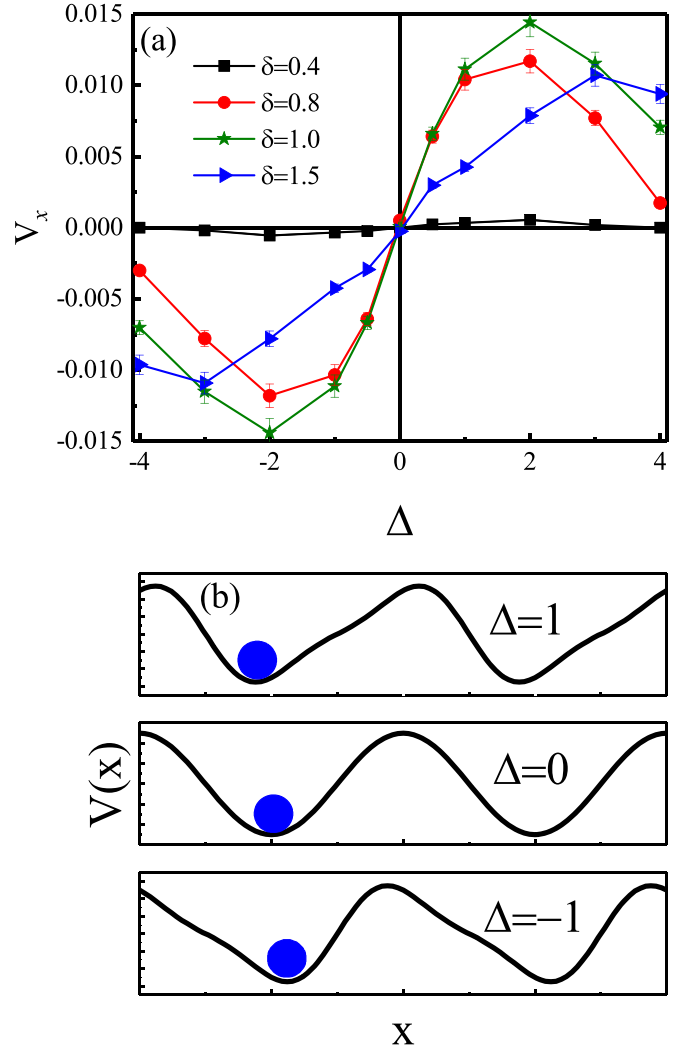


FIG. 3. (a) The average velocity  $V_x$  as a function of the asymmetric parameter  $\Delta$  of the potential for different  $\delta$  at  $\phi = 0.2$  and  $T = 0.3$ . (b) The profile of the potential  $V(x)$  along the  $x$  direction described in Eq. (2) for different values of the parameter  $\Delta$ . The left side of the potential is steep for  $\Delta > 0$  and the right side is steep for  $\Delta < 0$ . The error bars represent the standard deviation above and below the mean.

that nonreciprocal interactions between Brownian particles can significantly amplify their diffusivity, which is in line with findings from Ref. [60]. As  $\delta \rightarrow 0$ , the nonequilibrium driving force vanishes, rendering  $V_x$  negligible. Conversely, when  $\delta$  is significantly large, the nonequilibrium driving force  $f_x(t)$  intensifies to a substantial degree, enabling particles to traverse the potential barrier with such ease that its presence becomes almost imperceptible. Furthermore, the influence of the asymmetric potential becomes negligible, resulting in the rectifying effect being discounted, which subsequently reduces  $V_x$  to zero. Therefore, an optimal value for  $\delta$  exists, estimated to be at  $\delta = 1.0$ , where  $V_x$  reaches its maximum.

The dependence of the average velocity  $V_x$  on the temperature  $T$  is shown in Fig. 5(a) for different  $\delta$  at  $\phi = 0.2$  and  $\Delta = 2.0$ . Analogous to Fig. 4(a), the average velocity  $V_x$  exhibits a peak function in relation to  $T$ . As  $T$  tends

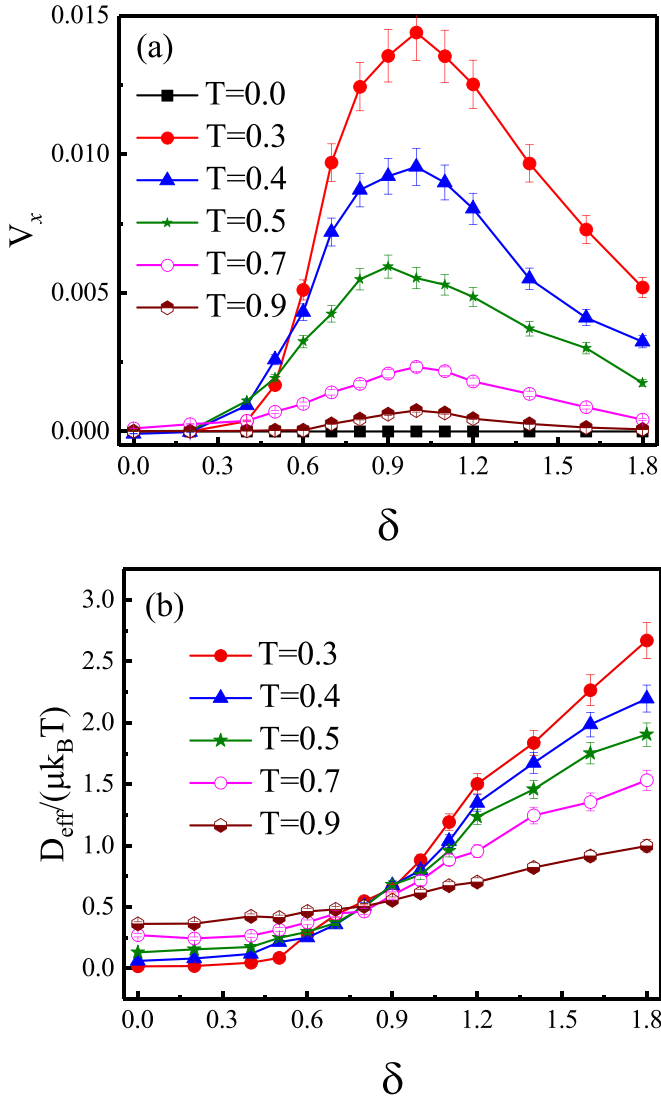


FIG. 4. (a) The average velocity  $V_x$  as a function of  $\delta$  for different  $T$ . (b) The effective diffusion coefficient  $D_{\text{eff}}/(\mu k_B T)$  as a function of  $\delta$  for different  $T$ . The other parameters are  $\phi = 0.2$  and  $\Delta = 2.0$ .

to zero, particles encounter difficulties in overcoming the potential barrier, causing  $V_x$  to approach zero. Directed motion is only accomplished when the temperature exceeds a specific threshold. This facilitates the nonequilibrium drive and noise in aiding the particle to cross the potential barrier. Conversely, when  $T$  approaches infinity, the potential barrier becomes negligible, the asymmetric potential's effect ceases, and no directional movement is produced, leading  $V_x$  to zero. Consequently, there exists an optimal value of  $T$  at which the rectification of the particle is maximized. Furthermore, as  $\delta$  increases, there is a marginal shift in the peak positions of the curves toward a smaller  $T$ .

In order to thoroughly investigate the interdependence of the average velocity  $V_x$  on  $\delta$  and  $T$ , a phase diagram was constructed. This diagram, illustrated in Fig. 5(b), emphasizes the average velocity in the  $\delta$ - $T$  representation at  $\phi = 0.2$  and  $\Delta = 2.0$ . In regions where  $\delta < 0.4$  or  $T < 0.1$ , it is difficult for particles to overcome the potential barrier, leading to an observable lack of directional movement. Conversely, when

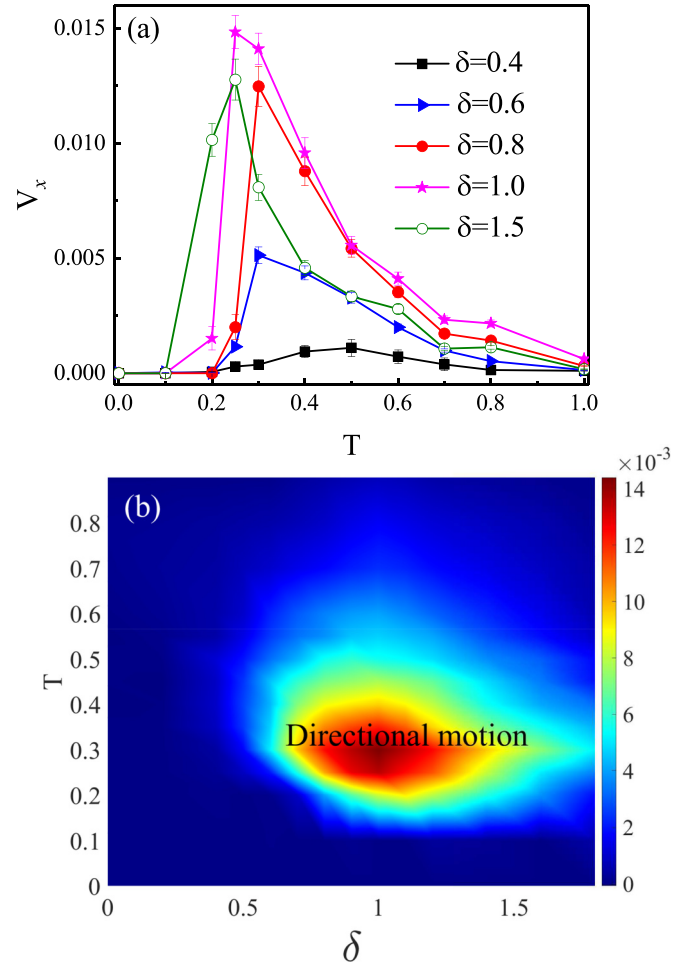


FIG. 5. (a) The average velocity  $V_x$  as a function of the temperature  $T$  for different  $\delta$ . (b) Phase diagram of the average velocity  $V_x$  in the  $\delta$ - $T$  representation. The other parameters are  $\Delta = 2.0$  and  $\phi = 0.2$ . The background represents the value of  $V_x$  according to the color bar on the right.

$T > 0.6$  or  $\delta > 2.0$ , particles can easily traverse the potential barrier, thereby resulting in the disappearance of asymmetric action and hence an absence of a rectification effect. This affirms the existence of an optimal parameter region for  $(\delta, T)$  where  $V_x$  attains its maximal value. The following discussion will elucidate the results. The degree of particle rectification is determined by the interplay between the driving force, dependent on  $T$  and  $\delta$ , and the potential barrier. A weak driving force cannot propel the particles over the potential barrier, resulting in the absence of directed motion. On the other hand, an excessively strong driving force can make the potential barrier insignificant, resulting in a loss of the asymmetry effect and thereby limiting directed motion. When the driving force exactly matches the potential barrier, creating a condition referred to as “directional motion” in the figure, optimal particle rectification is achieved.

We have also examined the relationship between the average velocity  $V_x$  and the temperature  $T$  for different values of  $\phi$ . This relationship is depicted in Fig. 6(a), and the range considered extends from the dilute regime to close packing ( $\phi_{cp} \approx 0.91$ ). We discovered that there exists a threshold temperature

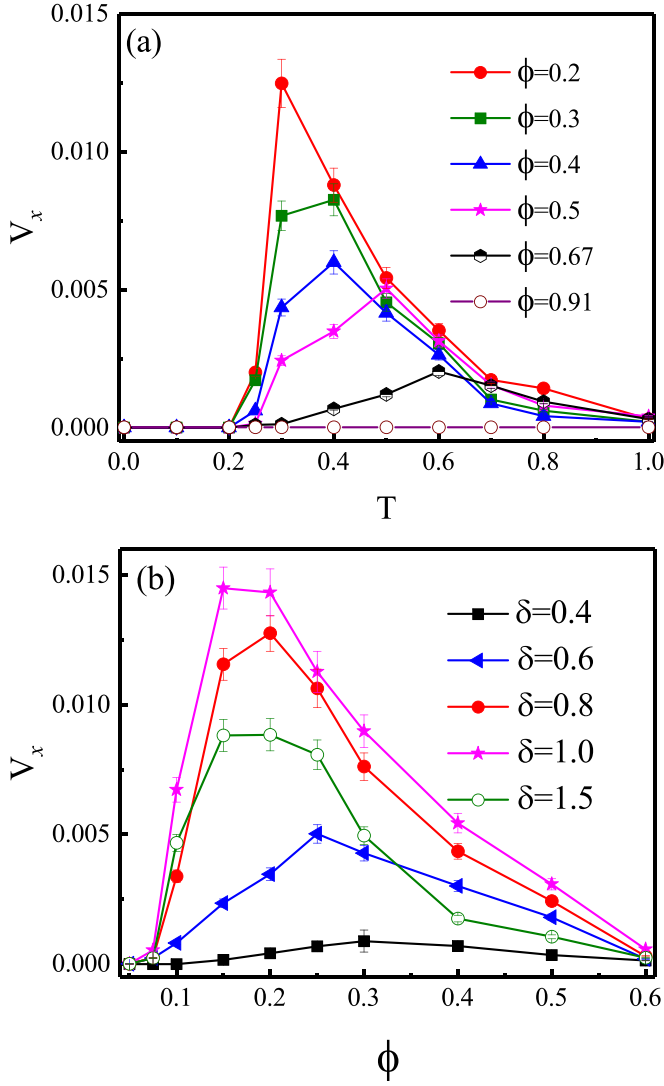


FIG. 6. (a) The average velocity  $V_x$  as a function of the temperature  $T$  For different  $\phi$  at  $\Delta = 2.0$  and  $\delta = 0.8$ . (b) The average velocity  $V_x$  as a function of the packing fraction  $\phi$  for different  $\delta$  at  $T = 0.3$  and  $\Delta = 2.0$ .

below which the average velocity  $V_x$  suddenly decreases. This phenomenon arises due to the formation of a dense phase at low temperatures. The thermal motions of the particles are insufficient to disrupt this phase, which hinders the particles from passing through the potential barrier, leading to zero net transport. Additionally, this threshold temperature increases with the rise in  $\phi$ . This can be attributed to the fact that a higher packing fraction facilitates the formation of a denser phase, demanding a higher temperature to destabilize it. Furthermore, an increase in  $\phi$  leads to a shift in the position of the peak in the curves toward higher temperatures. It is worth noting that when the density reaches a certain level (e.g.,  $\phi_{cp} \approx 0.91$ ), particle crystallization or jamming occurs, which leads to zero net transport.

Figure 6(b) illustrates the relationship between the average velocity  $V_x$  and the packing fraction  $\phi$  for varying values of  $\delta$  at a fixed  $T = 0.3$  and  $\Delta = 2.0$ . Noticeably, the average velocity displays a peaked function in relation to  $\phi$ . At

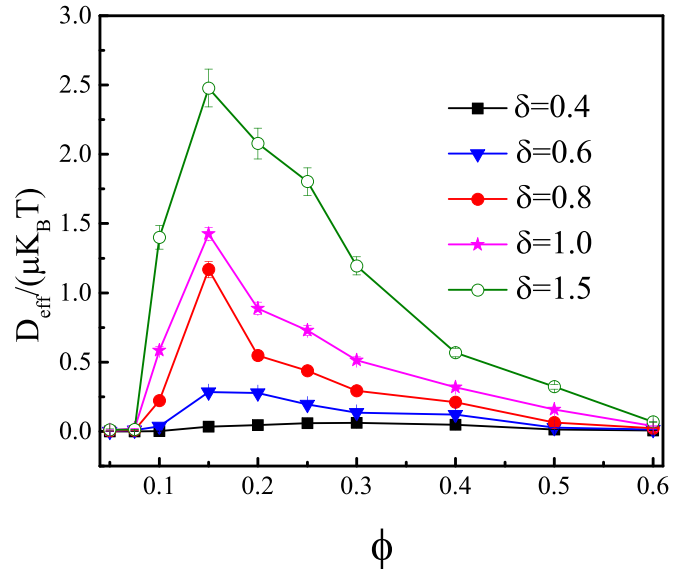


FIG. 7. The effective diffusion coefficient  $D_{\text{eff}}/(\mu k_B T)$  as a function of  $\phi$  for different  $\delta$  at  $T = 0.3$  and  $\Delta = 2.0$ .

extremely low  $\phi$  values, the particle density is minimal, thereby rendering interparticle interactions negligible. This condition induces the disappearance of the nonequilibrium drive, which is achieved by nonreciprocal interactions, consequently leading to the elimination of rectification. Conversely, when the packing fraction significantly increases, particle crowding becomes intense, ultimately reducing the average inter-particle indirect interaction to a marginal level, exemplified by  $r < 2^{1/6}\sigma$ . This scenario results in two primary effects: first, it causes the nonreciprocal part of the inter-particle force to vanish, eliminating the nonequilibrium drive. Second, it makes the rectification of particles inefficient due to overcrowding. Therefore, under high-density conditions, the average velocity tends to zero. Interestingly, there exists an optimal  $\phi$  at which  $V_x$  achieves its maximal value. Upon reviewing the curve peaks, it is apparent that their positions slightly shift toward smaller  $\phi$  values with escalating  $\delta$  levels.

Figure 7 illustrates the relationship between the effective diffusion and the packing fraction at  $T = 0.3$  and  $\Delta = 2.0$ . It is observed that the effective diffusion coefficient  $D_{\text{eff}}/(\mu k_B T)$  exhibits a peaked behavior with respect to the packing fraction  $\phi$ . This can be explained as follows: when particles are confined within a potential well, increasing the density has two distinct effects. Initially, at lower packing densities, it facilitates the particles' ability to overcome the potential barrier, thereby enhancing diffusion. However, at higher densities, the motion of the particles becomes more constrained, resulting in a decrease in diffusion. As the packing fraction  $\phi$  gradually increases from zero, the initial factors play a significant role, leading to an increase in  $D_{\text{eff}}/(\mu k_B T)$ . However, as the density becomes large enough for the particles to smoothly pass through the potential barrier, the subsequent factors become dominant, resulting in a decrease in  $D_{\text{eff}}/(\mu k_B T)$ . Consequently, there exists an optimal density at which the diffusion coefficient is maximized.

We explore the impact of the system size on the rectification of mixed Brownian particles, as depicted in Fig. 8, with

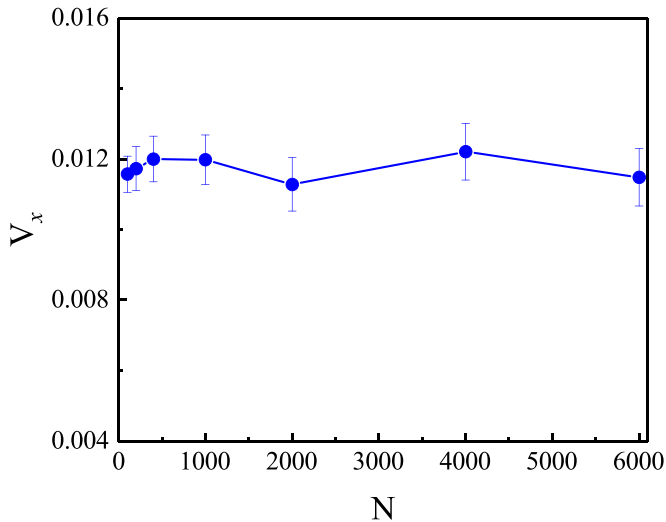


FIG. 8. The average velocity  $V_x$  as a function of the particle number  $N$  at  $\delta = 0.8$ ,  $\phi = 0.2$ ,  $T = 0.3$ , and  $\Delta = 2.0$ .

$T = 0.3$ ,  $\delta = 0.8$ , and  $\Delta = 2.0$ . We maintained a constant  $\phi = 0.2$ , while the system size ( $L_x$  and  $L_y$ ) adjusted in accordance with the total particle number  $N$ . Our findings indicate no significant deviations in the average velocity  $V_x$  as the particle number  $N$  changes. This suggests that the rectification of particles remains unaffected by the scale of the system.

Finally, we will briefly discuss the one-dimensional case. For particles with no bias in their position distribution, we obtained similar results to those of the two-dimensional case (which are not presented here). However, there are the following differences in the one-dimensional case. In the one-dimensional case, particles are unable to pass through each other, resulting in each particle having fixed neighbors that remain unchanged over time, leading to a single-file motion. For instance, a biased particle distribution propels a force that deviates from the conventional random force with zero mean, displaying a skewed random force instead. Additionally, the diffusion behavior of the particles is significantly reduced compared to the two-dimensional scenario, due to the single-file motion.

#### IV. CONCLUSION AND OUTLOOK

In this paper, we studied the directed transport of mixed Brownian particles with nonreciprocal interactions in a

two-dimensional periodic asymmetric potential. It was discovered that such interactions could induce an interaction-dependent nonequilibrium drive, which is dependent on both the configurations of the particles and the degree of nonreciprocity. This externally introduced force can break the system's thermodynamic equilibrium and induce the directed motion of Brownian particles within an asymmetric periodic potential. The direction of this motion is determined by the asymmetry of the potential. The average velocity presents as positive for  $\Delta > 0$ , zero at  $\Delta = 0$ , and negative for  $\Delta < 0$ . Moreover, the average velocity exhibits a peak function with the degree of nonreciprocity, while the effective diffusion coefficient consistently increases with an increase in nonreciprocity. There exists a distinct optimal packing fraction or temperature at which the maximum average velocity can be attained. Importantly, these findings maintain applicability and are not exclusive to any finite size effects.

In the traditional ratchet model, a particle-autonomous nonequilibrium drive is essential, with the interactions between particles adhering to Newton's Third Law. In this context, we propose a method for rectifying Brownian particles using an interaction-dependent nonequilibrium drive, propelled by nonreciprocal interactions. This alleviates the need for a particle-autonomous nonequilibrium drive. Concurrently, we propose a strategy for transposing the energy of nonreciprocal interactions into directed motion. It should be noted that in binary particle mixtures with nonreciprocal interactions, like the one investigated in our study, net currents (with randomly selected directions) can be achieved without the requirement of an external potential [56,70,71]. This phenomenon arises from the spontaneously emerging current inherent to the nonreciprocal binary mixture, in conjunction with the broken spatial asymmetry induced by the potential. At present, this is merely a theoretical concept and the validation of its application should be pursued through laboratory experiments on nonreciprocal systems [63,64,66]. This could significantly impact our understanding of the complex behaviors observed in various out-of-equilibrium systems.

#### ACKNOWLEDGMENTS

This work was supported in part by the National Natural Science Foundation of China (Grant No. 12075090), the Key-Area Research and Development Program of Guangdong Province (Grant No. 2019B030330001), and the Natural Science Foundation of Guangdong Province (Grant No. 2022A1515010449).

- 
- [1] G. Oster, *Nature (London)* **417**, 25 (2002).
  - [2] H. Noji, R. Yasuda, M. Yoshida, and K. Kinoshita Jr., *Nature (London)* **386**, 299 (1997).
  - [3] J. C. M. Kistemaker, P. Štacko, D. Roke, A. T. Wolters, G. H. Heideman, M.-C. Chang, P. van der Meulen, J. Visser, E. Otten, and B. L. Feringa, *J. Am. Chem. Soc.* **139**, 9650 (2017).
  - [4] W. R. Wilson, J. Solà, A. Carlone, S. M. Goldup, N. Lebrasseur, and D. A. Leigh, *Nature (London)* **534**, 235 (2016).
  - [5] R. D. Astumian, *Science* **276**, 917 (1997).
  - [6] J. Rousselet, L. Salome, A. Ajdari, and J. Prost, *Nature (London)* **370**, 446 (1994).
  - [7] R. D. Astumian and P. Hänggi, *Phys. Today* **55**(11), 33 (2002).
  - [8] P. Hänggi and F. Marchesoni, *Rev. Mod. Phys.* **81**, 387 (2009).
  - [9] P. Reimann, *Phys. Rep.* **361**, 57 (2002).
  - [10] C. J. Olson Reichhardt and C. Reichhardt, *Annu. Rev. Condens. Matter Phys.* **8**, 51 (2017).
  - [11] M. O. Magnasco, *Phys. Rev. Lett.* **71**, 1477 (1993).

- [12] R. Bartussek, P. Reimann, and P. Hänggi, *Phys. Rev. Lett.* **76**, 1166 (1996).
- [13] C. Grossert, M. Leder, S. Denisov, P. Hänggi, and M. Weitz, *Nat. Commun.* **7**, 10440 (2016).
- [14] Y.-F. He, B.-Q. Ai, C.-X. Dai, C. Song, R.-Q. Wang, W.-T. Sun, F.-C. Liu, and Y. Feng, *Phys. Rev. Lett.* **124**, 075001 (2020).
- [15] B.-Q. Ai and L.-G. Liu, *Phys. Rev. E* **74**, 051114 (2006).
- [16] B.-Q. Ai, *Phys. Rev. E* **96**, 012131 (2017).
- [17] B.-Q. Ai, J. Ma, C.-H. Zeng, and Y.-F. He, *Phys. Rev. E* **107**, 024406 (2023).
- [18] Y. Li, P. K. Ghosh, F. Marchesoni, and B. Li, *Phys. Rev. E* **90**, 062301 (2014).
- [19] J. Bang, R. Pan, T. M. Hoang, J. Ahn, C. Jarzynski, H. T. Quan, and T. C. Li, *New J. Phys.* **20**, 103032 (2018).
- [20] G. Camacho, A. Rodriguez-Barroso, O. Martinez-Cano, J. R. Morillas, P. Tierno, and J. de Vicente, *Phys. Rev. Appl.* **19**, L021001 (2023).
- [21] A. Gnoli, A. Petri, F. Dalton, G. Pontuale, G. Gradenigo, A. Sarracino, and A. Puglisi, *Phys. Rev. Lett.* **110**, 120601 (2013).
- [22] D. Cubero and F. Renzoni, *Phys. Rev. Lett.* **116**, 010602 (2016).
- [23] C. Schwemmer, S. Fringes, U. Duerig, Y. K. Ryu, and A. W. Knoll, *Phys. Rev. Lett.* **121**, 104102 (2018).
- [24] R. D. Astumian and M. Bier, *Phys. Rev. Lett.* **72**, 1766 (1994).
- [25] M. Borromeo and F. Marchesoni, *Phys. Lett. A* **249**, 199 (1998).
- [26] B. Lau, O. Kedem, M. A. Ratner, and E. A. Weiss, *Phys. Rev. E* **93**, 062128 (2016).
- [27] C. Sándor, A. Libál, C. Reichhardt, and C. J. Olson Reichhardt, *Phys. Rev. E* **95**, 012607 (2017).
- [28] V. M. Rozenbaum, Y. A. Makhnovskii, I. V. Shapochkina, S.-Y. Sheu, D.-Y. Yang, and S. H. Lin, *Phys. Rev. E* **89**, 052131 (2014).
- [29] N. E. Strand, R.-S. Fu, and T. R. Gingrich, *Phys. Rev. E* **102**, 012141 (2020).
- [30] I. Derényi and T. Vicsek, *Phys. Rev. Lett.* **75**, 374 (1995).
- [31] Z. Zheng, G. Hu, and B. Hu, *Phys. Rev. Lett.* **86**, 2273 (2001).
- [32] C. C. de Souza Silva, J. Van de Vondel, M. Morelle, and V. V. Moshchalkov, *Nature (London)* **440**, 651 (2006).
- [33] D. Mei, C. Xie, and L. Zhang, *Phys. Rev. E* **68**, 051102 (2003).
- [34] R. L. Stoop, A. V. Straube, T. H. Johansen, and P. Tierno, *Phys. Rev. Lett.* **124**, 058002 (2020).
- [35] C. Roberts and Z. Zhen, *Phys. Rev. E* **108**, 014139 (2023).
- [36] R. Di Leonardo, L. Angelani, D. Dell'Arciprete, G. Ruocco, V. Iebba, S. Schippa, M. P. Conte, F. Mecarini, F. De Angelis, and E. Di Fabrizio, *Proc. Natl. Acad. Sci. USA* **107**, 9541 (2010).
- [37] A. K. Pumm, W. Engelen, E. Kopperger, J. Isensee, M. Vogt, V. Kozina, M. Kube, M. N. Honemann, E. Bertolin, M. Langecker, R. Golestanian, F. C. Simmel, and H. Dietz, *Nature (London)* **607**, 492 (2022).
- [38] M. B. Wan, C. J. Olson Reichhardt, Z. Nussinov, and C. Reichhardt, *Phys. Rev. Lett.* **101**, 018102 (2008).
- [39] L. Angelani, R. Di Leonardo, and G. Ruocco, *Phys. Rev. Lett.* **102**, 048104 (2009).
- [40] P. K. Ghosh, V. R. Misko, F. Marchesoni, and F. Nori, *Phys. Rev. Lett.* **110**, 268301 (2013).
- [41] P. K. Ghosh, P. Hänggi, F. Marchesoni, and F. Nori, *Phys. Rev. E* **89**, 062115 (2014).
- [42] F. Kümmel, B. ten Hagen, R. Wittkowski, I. Buttinoni, R. Eichhorn, G. Volpe, H. Lowen, and C. Bechinger, *Phys. Rev. Lett.* **110**, 198302 (2013).
- [43] A. Kaiser, A. Peshkov, A. Sokolov, B. ten Hagen, H. Löwen, and I. S. Aranson, *Phys. Rev. Lett.* **112**, 158101 (2014).
- [44] A. Pototsky, A. M. Hahn, and H. Stark, *Phys. Rev. E* **87**, 042124 (2013).
- [45] D. McDermott, C. J. Olson Reichhardt, and C. Reichhardt, *Soft Matter* **12**, 8606 (2016).
- [46] F. Q. Potiguar, G. A. Farias, and W. P. Ferreira, *Phys. Rev. E* **90**, 012307 (2014).
- [47] J. A. Drocco, C. J. Olson Reichhardt, and C. Reichhardt, *Phys. Rev. E* **85**, 056102 (2012).
- [48] G. Lambert, D. Liao, and R. H. Austin, *Phys. Rev. Lett.* **104**, 168102 (2010).
- [49] C. Reichhardt, D. Ray, and C. J. Olson Reichhardt, *New J. Phys.* **17**, 073034 (2015).
- [50] I. Berdakin, Y. Jeyaram, V. V. Moshchalkov, L. Venken, S. Dierckx, S. J. Vanderleyden, A. V. Silhanek, C. A. Condat, and V. I. Marconi, *Phys. Rev. E* **87**, 052702 (2013).
- [51] P. Kalinay and F. Slanina, *Phys. Rev. E* **108**, 014606 (2023).
- [52] M. Muhsin and M. Sahoo, *Phys. Rev. E* **107**, 054601 (2023).
- [53] J.-J. Liao, W.-J. Zhu, and B.-Q. Ai, *Phys. Rev. E* **97**, 062151 (2018).
- [54] B.-Q. Ai, Q.-Y. Chen, Y.-F. He, F.-G. Li, and W.-R. Zhong, *Phys. Rev. E* **88**, 062129 (2013).
- [55] B.-Q. Ai, Y.-F. He, and W.-R. Zhong, *Phys. Rev. E* **95**, 012116 (2017).
- [56] Z. You, A. Baskaran, and M. C. Marchetti, *Proc. Natl. Acad. Sci. USA* **117**, 19767 (2020).
- [57] Y.-J. Chiu and A. K. Omar, *J. Chem. Phys.* **158**, 164903 (2023).
- [58] A. V. Ivlev, J. Bartnick, M. Heinen, C.-R. Du, V. Nosenko, and H. Löwen, *Phys. Rev. X* **5**, 011035 (2015).
- [59] R. Mandal, S. S. Jaramillo, and P. Sollich, [arXiv:2212.05618](https://arxiv.org/abs/2212.05618).
- [60] A. Benois, M. Jardat, V. Dahirel, V. Démery, J. Agudo-Canalejo, R. Golestanian, and P. Illien, [arXiv:2307.05408](https://arxiv.org/abs/2307.05408).
- [61] K. L. Kreienkamp and S. H. L. Klapp, *New J. Phys.* **24**, 123009 (2022).
- [62] R. K. Gupta, R. Kant, H. Soni, A. K. Sood, and S. Ramaswamy, *Phys. Rev. E* **105**, 064602 (2022).
- [63] C. H. Meredith, P. G. Moerman, J. Groenewold, Y.-J. Chiu, W. K. Kegel, A. van Blaaderen, and L. D. Zarzar, *Nat. Chem.* **12**, 1136 (2020).
- [64] R. A. Long and F. Azam, *Appl. Environ. Microbiol.* **67**, 4975 (2001).
- [65] A. Strandburg-Peshkin, C. R. Twomey, N. W. F. Bode, A. B. Kao, Y. Katz, C. C. Ioannou, S. B. Rosenthal, C. J. Torney, H. S. Wu, S. A. Levin, and I. D. Couzin, *Curr. Biol.* **23**, R709 (2013).
- [66] G. Gardi and M. Sitti, *Phys. Rev. Lett.* **131**, 058301 (2023).
- [67] L. Cocconi, H. Alston, and T. Bertrand, [arXiv:2304.07738](https://arxiv.org/abs/2304.07738).
- [68] J. E. Lennard-Jones, *Proc. R. Soc. A* **106**, 463 (1924).
- [69] S. A. M. Loos and S. H. L. Klapp, *New J. Phys.* **22**, 123051 (2020).
- [70] S. Saha, J. Agudo-Canalejo, and R. Golestanian, *Phys. Rev. X* **10**, 041009 (2020).
- [71] T. Suchanek, K. Kroy, and S. A. M. Loos, [arXiv:2303.16701](https://arxiv.org/abs/2303.16701).